

Electronic Supplementary Information (ESI)

Ruthenium-based Plasmonic Hybrid Photocatalyst for Aqueous Carbon Dioxide Conversion with High Reaction Rate and Selectivity

Hwiseok Jun[†], Shinyoung Choi[†], Moon Young Yang^{‡,*}, and Yoon Sung Nam^{†,‡,*}

[†] Department of Materials Science and Engineering, Korea Advanced Institute of Science and Technology, Daejeon 34141, Republic of Korea

[‡] KAIST Institute for NanoCentury, Korea Advanced Institute of Science and Technology, Daejeon 34141, Republic of Korea

Corresponding Authors

* E-mail: yoonsung@kaist.ac.kr (Y.S.N.) and yangmy@kaist.ac.kr (M.Y.Y.)

Contents

1. Fabrication of half-dome-shaped Au/TiO ₂ heterostructure on ITO substrate	3
2. Synthesis of <i>cis</i> -dichloro-(4,4'-diphosphonato-Rubpy)(<i>p</i> -cymene) (RuCY)	3
3. Homogeneous electrocatalytic analysis	4
4. Photocatalytic CO ₂ reduction	4
5. Calculation of CO ₂ concentration in solvents	5
6. Computational calculations	6
Figure S1. Schematic drawing of RuCY preparation	7
Figure S2. ¹ H-NMR spectrum of RuCY in DMSO-d ₆	7
Figure S3. Normalized absorption spectra of the ruthenium complex precursor and RuCY (left), and the HOMO-LUMO energy gap of RuCY (right)	8
Figure S4. The calculated energy level diagrams and molecular orbitals for the precursor-dimer and RuCY	9
Figure S5. Electrochemical analysis data and chemical structures	10
Figure S6. Fabrication process of the Au/TiO ₂ half-dome structure	11
Figure S7. Absorption spectra: TiO ₂ , Au/TiO ₂ , and Au/TiO ₂ /RuCY	12
Figure S8. GC chromatograms of formic acid, methanol, H ₂ , and deionized water.....	12
Figure S9. Catalytic activity according to the TEOA concentration	13
Table S1. The catalytic activity of Au/TiO ₂ , TiO ₂ /RuCY, and Au/TiO ₂ /RuCY in the same reaction condition	14
Table S2. Summary of previous researches on CO ₂ reduction in photocatalytic systems using Ru-based molecular catalysts	15
Figure S10. The amount of Ru atom after the reaction under 243 mW·cm ⁻²	16
Figure S11. Increased reaction rate in acetone-added solvents	17
Figure S12. Structure of the transition state of proton insertion step	18
Table S3. The amount and selectivity of reduction products in 5 different light intensities.....	19
References	20

1. Fabrication of half-dome-shaped Au/TiO₂ heterostructure on ITO substrate

ITO-coated glass slides were cleaned by ultra-sonication (SK7200BT, Youngjin Corporation) for 15 min in acetone and methanol, respectively. Photoresist patterns were fabricated on the substrates by conventional photolithography. HMDS was spin-coated as an adhesion promoter and AZ-GXR 601 was used as a photoresist. After UV exposure by mask aligner (MIDAS-1600), the cylindrical photoresist pattern (diameter: 2 μm and spacing: 2 μm) was fabricated by a developing process (developer: AZ-300MIF). Au (20 nm) and TiO₂ (10 nm) thin films were evaporated in series on the photoresist patterns by e-beam evaporation (E-beam evaporator-150S, A-Tech system). Thin film layers were deposited on the side of the photoresist cylinders because the substrates were oblique at an angle of 60°. Au/TiO₂ half-dome heterostructures were left by following lift-off process with acetone. Then, the molecular catalyst (0.2 mg·mL⁻¹ in DMSO) was immobilized onto the surface of TiO₂ with shaking incubation at room temperature over 12 h.

2. Synthesis of *cis*-dichloro-(4,4'-diphosphonato-Rubpy)(*p*-cymene) (RuCY)

RuCY was synthesized following previous literatures with modifications.^{1,2} 4,4'-Dibromo-2,2'-bipyridine solution (0.3 M) in anhydrous toluene was magnetically stirred for 20 min with argon purging. Another 10 min of stirring was carried out after 2.5 equivalents of diethyl phosphite and 3 equivalents of triethylamine were slowly injected. After the designated time, under positive outward pressure by argon gas, 5 mol% of *tetrakis*-(triphenylphosphine) palladium was added into the mixture, and three more hours of reaction was performed at 80-90 °C. The process of the reaction was monitored by thin-layer chromatography eluted by 4:4:1 solution of toluene/heptane/triethylamine. When the reaction was terminated, the mixture was put into a silica gel column for flash chromatography by the same solution of toluene/heptane/triethylamine. The solid product was dissolved again in pure acetonitrile, and dichloro-(*p*-cymene) ruthenium (II) dimer was suspended into the solution. The heterogeneous

suspension was bubbled by Ar for 20 min. Then, the mixture was refluxed for 4 h, and the colour of the mixture became dark during the process. When the time is over, the pot was placed in a 4°C refrigerator over 6 to 12 h to precipitate enough the suspended brown product. The precipitate was filtered and washed 3 times with cold acetonitrile. The obtained solid was dried in a 40°C vacuum oven over 6 hours to give *cis*-dichloro-(4,4'-bis(diethylphosphonato)-Rubpy)(*p*-cymene), the precursor of the desired molecular catalyst. The precursor was dissolved in 1:1 solution of anhydrous acetonitrile and dichloromethane, and 2.2 equivalent of bromotriethylsilane was added carefully in a highly inert-gas environment. The reaction mixture was refluxed over 12 h and cooled down to ambient temperature. The product was obtained by precipitation with slow addition of cold water into the mixture. The solid was filtered and washed with cold water several times, and dried in a 40°C vacuum oven over 6 h to give *cis*-dichloro-(4,4'-diphosphonato-Rubpy)(*p*-cymene). The structure of the final molecular catalyst was assigned by proton-NMR. ¹H-NMR (300 MHz, DMSO-d₆, δ): 9.59 (2H, d), 7.86 (2H, d), 7.13 (2H, dd), 6.25 (2H, d), 6.01 (2H, d), 2.62 (1H, m), 2.17 (3H, s), 0.95 (6H, d)

3. Homogeneous electrocatalytic analysis

This test was consisted of a three-electrode configuration in acetate buffer at pH 3.7 or 3.0 at a scan rate of 100 mV s⁻¹ for 15 cycles. Glassy carbon, Pt wires, and Ag/AgCl were used as working, counter, and reference electrodes, respectively. The electronic potentials were converted into the reversible hydrogen electrode (RHE) scale using the following equation;

$$E_{(\text{RHE})} = E_{(\text{Ag}/\text{AgCl})} + 0.059 \times \text{pH} + E_{(\text{Ag}/\text{AgCl})}^0, \text{ where } E_{(\text{Ag}/\text{AgCl})}^0 = 0.197 \text{ V at } 25^\circ\text{C}.$$

4. Photocatalytic CO₂ reduction

The aqueous electrolyte solutions were sodium acetate/acetic acid buffer for pH 3, 3.7, and 4.8, and $\text{KH}_2\text{PO}_4/\text{Na}_2\text{HPO}_4$ buffer for pH 5.8 and 6.3. Each buffer solution contained 0.2 M triethanolamine (TEOA) (Sigma-Aldrich). The electrolyte solutions were degassed under reduced pressure and Ar bubbling, and then the buffered solution was saturated with CO_2 by bubbling in slightly positive pressure for 1 hour. RuCY-loaded Au/ TiO_2 photocatalyst was put in a 5 mL vial containing 2.5 mL of buffered solution, and the gas phase was replaced and purged with Ar while the vial is tightly sealed with a rubber septum and paraffin seal-tape. The vial was placed in front of 300 W or 450 W Xenon lamp, and the light was irradiated for designated periods of time with a 400 nm long-pass filter. Chemical species in the aqueous and gas phases were determined respectively by gas chromatography (YL6500 GC system, carrier gas: helium, flow rate: $1.0 \text{ mL}\cdot\text{min}^{-1}$, detector: TCD for gas phase, PDD for aqueous phase, column for TCD: SUPELCO Analytical, Mol Sieve 5A, 6 ft \times 1/8 inch, column for PDD: Agilent Technologies, HP-FFAP, 30 m \times 0.53 mm, 1.00 μm).

5. Calculation of CO_2 concentration in solvents

The saturated concentrations of CO_2 in water or acetone were calculated by following a literature which reports the solubility of CO_2 in various solvents.³ The literature describes the number of molecules of a solvent required to dissolve CO_2 . According to the result, 1,350 molecules of water or 46 molecules of acetone are required to dissolve one molecule of CO_2 . Due to the molarity of water and acetone are 55.4 and 13.5, respectively, 41 mM of CO_2 is dissolved in water, and 293 mM of CO_2 is dissolved in acetone at 20°C. Therefore, the following brief calculations can be derived.

for water,

$$[\text{CO}_2] = 41 \text{ mM}$$

for water:acetone = 7:3 solvent,

$$[\text{CO}_2] = (41 \text{ mM} \times 0.7) + (293 \text{ mM} \times 0.3) = 117 \text{ mM}$$

for water:acetone = 3:7 solvent,

$$[\text{CO}_2] = (41 \text{ mM} \times 0.3) + (293 \text{ mM} \times 0.7) = 218 \text{ mM}$$

6. Computational calculations

All geometries were fully optimized at the M06-L level of density functional theory with the Gaussian 09 electronic structure program suite using the LanL2DZ pseudopotential basis set for the Ru atom and the MIDI! basis set for all other atoms.⁴⁻⁷ The energies were subsequently computed with a larger basis set using the same basis set on Ru, but the 6-311+G(2df,2p) basis set on all other atoms. The nature of all stationary points was verified by analytical computation of vibrational frequencies, which were also used for the computation of zero-point vibrational energies and molecular partition functions for use in computing 298 K thermal contributions to enthalpies. Solvent effects of water were included with the SMD continuum solvation model.⁸

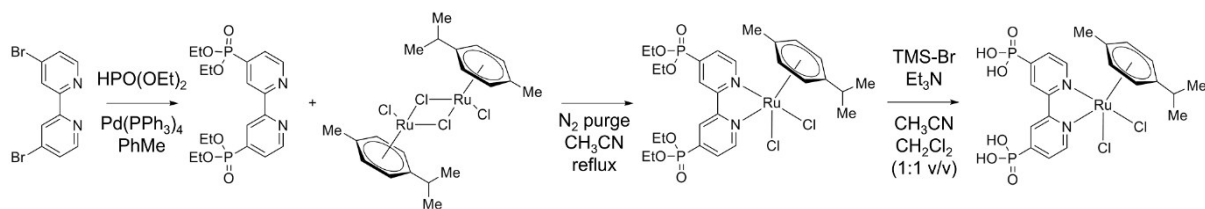


Figure S1. Schematic drawing of RuCY preparation.

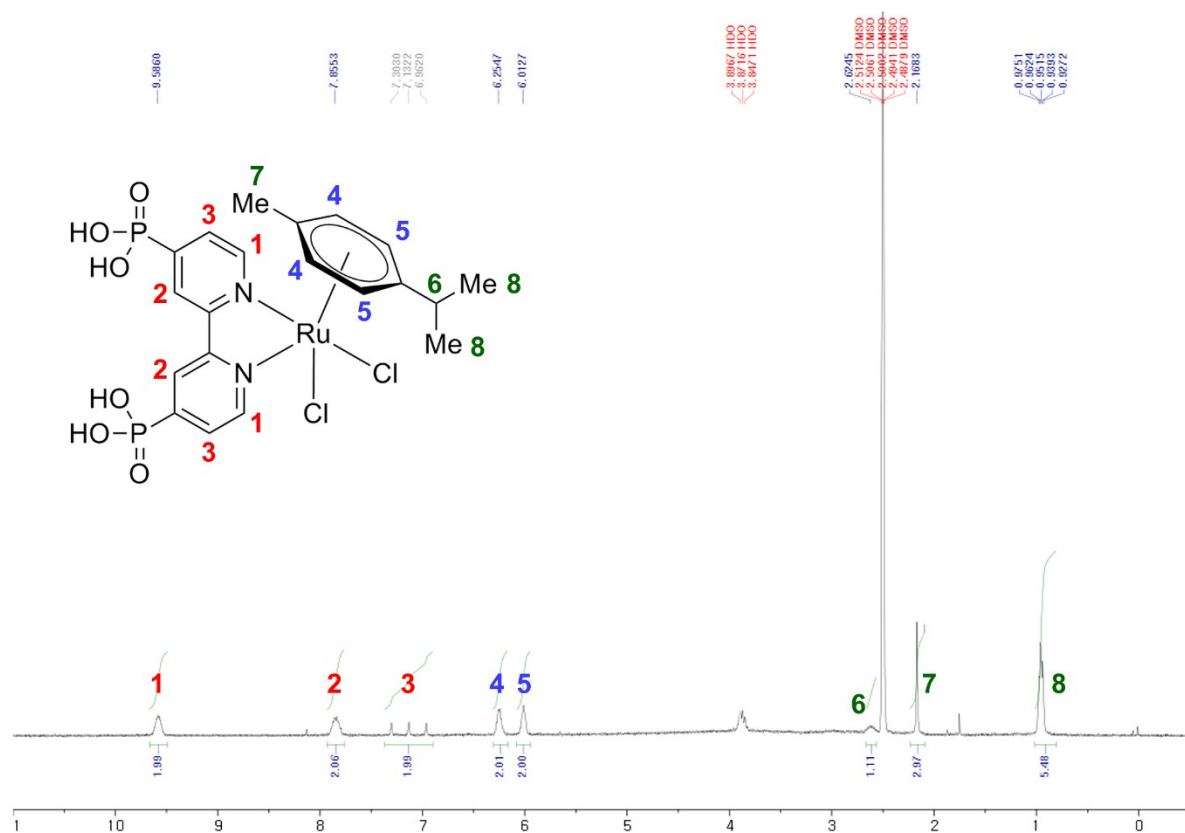


Figure S2. $^1\text{H-NMR}$ spectrum of RuCY in DMSO-d_6 .

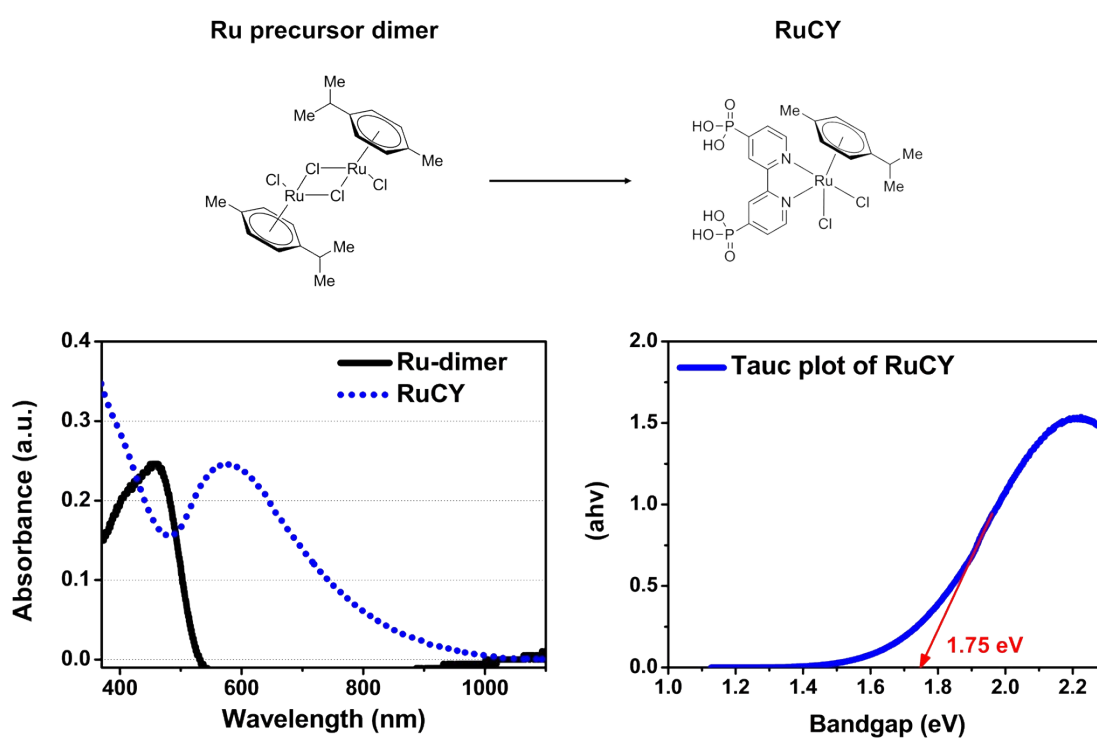


Figure S3. Normalized absorption spectra of the ruthenium complex precursor and RuCY (left), and the HOMO-LUMO energy gap of RuCY (right).

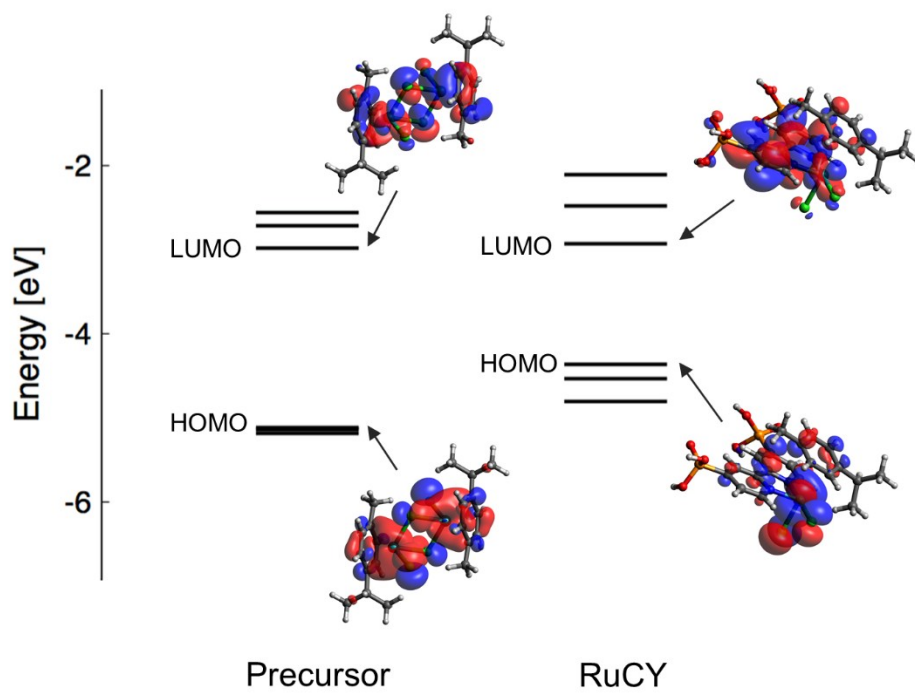


Figure S4. The calculated energy level diagrams and molecular orbitals for the precursor-dimer and RuCY.

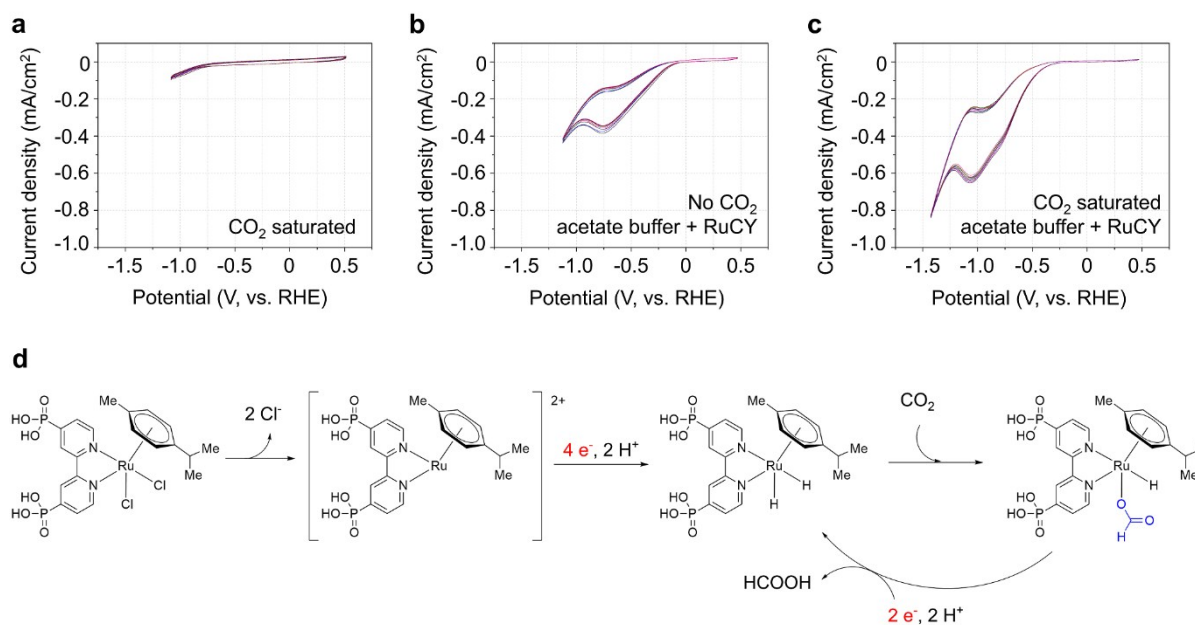


Figure S5. Cyclic voltammograms of (a) the CO₂-saturated aqueous solution in pH 3.7, (b) degassed and Ar-purged acetate buffer solution (pH 3) with dissolved RuCY in 0.5 mM, and (c) the same acetate buffer solution contains both CO₂ and RuCY scanned at 100 mV/s for 15 cycles. (d) The chemical structures of RuCY corresponding to the electrochemical process.

WE: Glassy carbon, CE: Pt wire, RE: Ag/AgCl (sat. KCl).

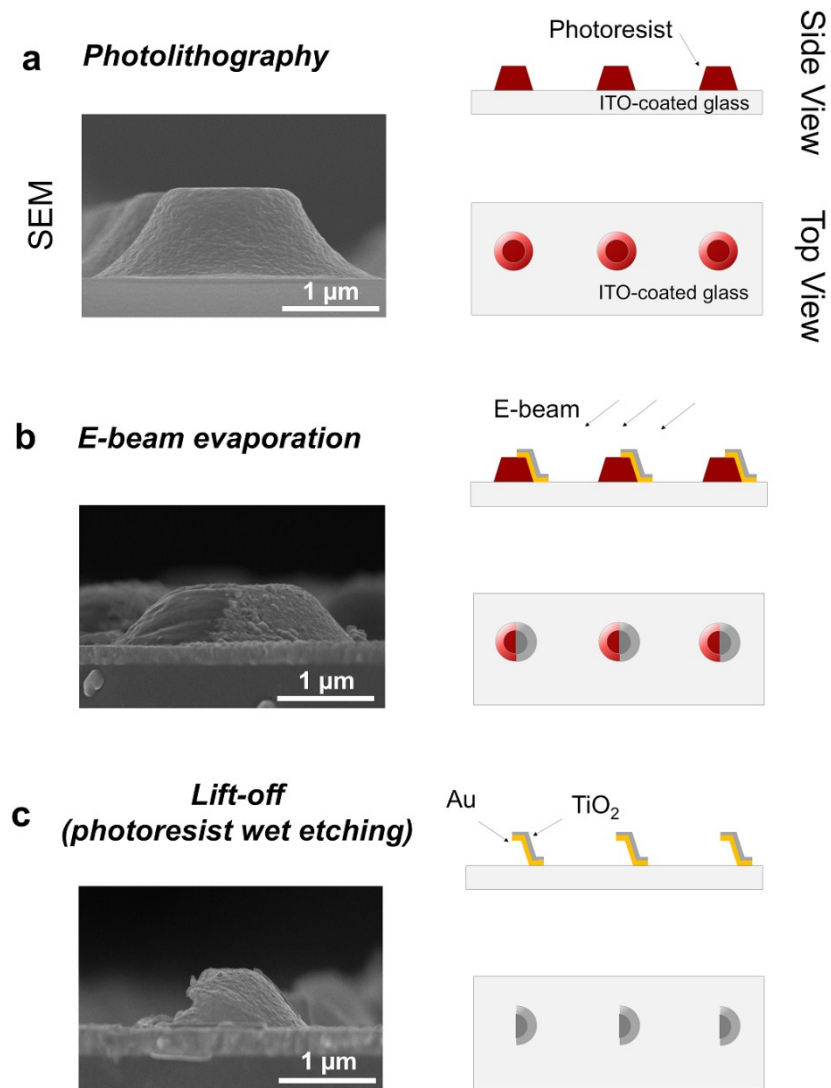


Figure S6. Fabrication process of the half-dome-shaped, plasmonic Au/TiO₂ heterostructures through (a) photolithography, (b) e-beam lithography, and (c) lift-off of photoresist by wet etching in acetone.

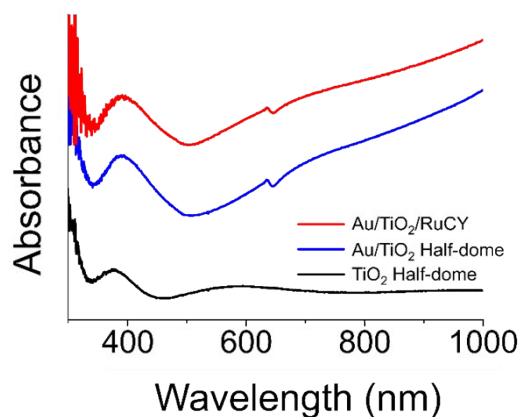


Figure S7. Absorption spectra of TiO₂ half-dome, Au/TiO₂ half-dome, and Au/TiO₂ half-dome/RuCY photocatalyst. (Given the arbitrary offset in Y axis to increase readability)

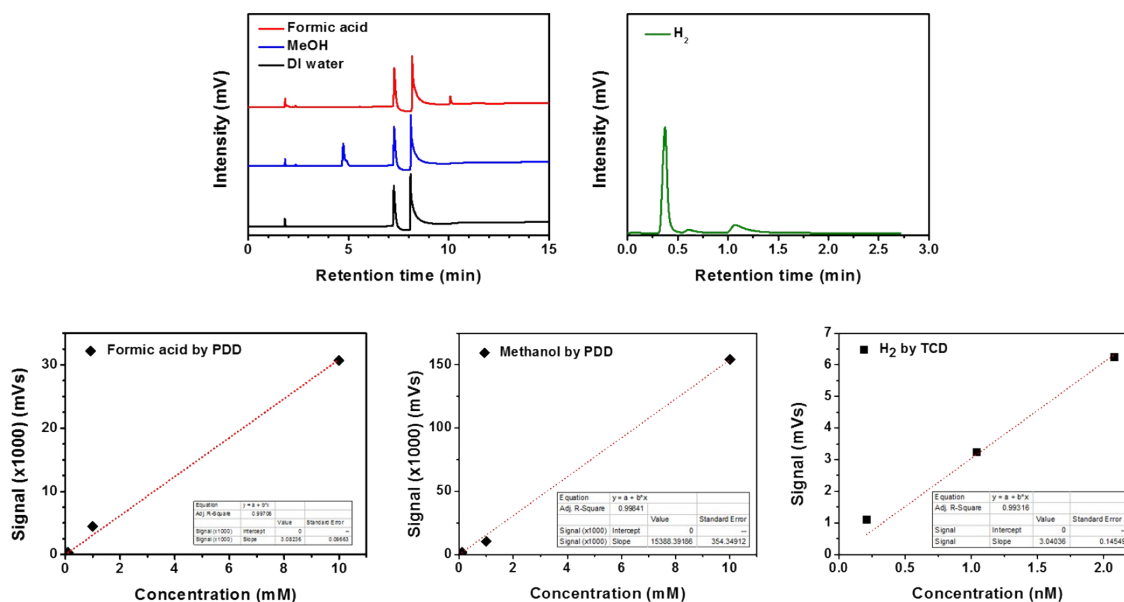


Figure S8. GC chromatograms of formic acid (red line), methanol (blue line), H₂ (green line), deionized water (black line), and their calibration curves. Carrier gas = helium; flow rate = 1.0 mL min⁻¹; and detector = PDD for formic acid and methanol, and TCD for H₂.

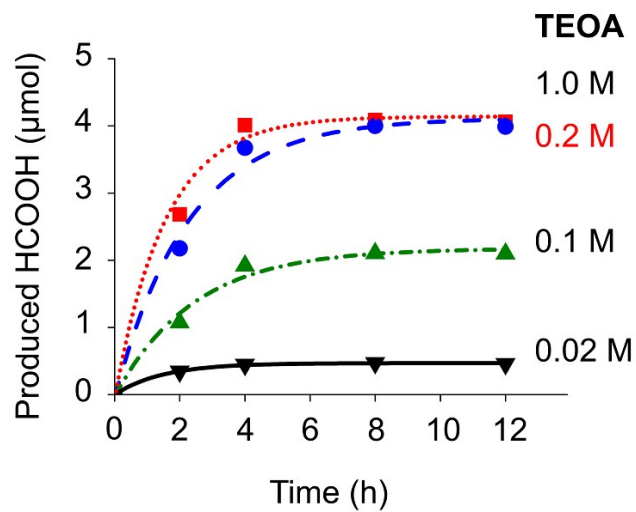


Figure S9. The amount of produced formic acid during the reaction per 3.11 nmol of RuCY in different concentrations of TEOA. The advanced reactivity didn't appeared after 0.2 M.

Table S1. The catalytic activity of Au/TiO₂, TiO₂/RuCY, and Au/TiO₂/RuCY in the same reaction condition.

Product	Amount (nmol)			
	Blank	Au/TiO₂	TiO₂/RuCY^{a)}	Au/TiO₂/RuCY^{a)}
Formic acid	0	0	0	1245.4
Methanol	0.4	0.6	0.4	32.8
Hydrogen	2.0	4.5	1.4	1.2
CO	0	0	0	0

a) Reaction condition: Electrolyte = acetate buffer pH 3 containing 0.2 M TEOA; loaded RuCY = 1 nmol; reaction time = 2 h; and light intensity = 243 mW·cm⁻².

Table S2. Summary of previous researches on CO₂ reduction in photocatalytic systems using Ru-based molecular catalysts.

Light source	Catalyst	Reaction medium	Major Products (% selectivity)	Performance ^{a)}	Ref
Mercury (Hg) lamp >320 nm	Ru(bpy) ₂ (CO) ₂	DMF/water (9:1)	CO (78 %)	Φ= 0.14 TOF= 19 h ⁻¹ TON= 372	9
Halogen lamp >400 nm	<i>cis</i> -Ru(bpy) ₂ L ₂	DMF/TEOA (4:1)	Formic acid (42 %)	Φ= 0.15 TOF= 163 h ⁻¹ TON= 326	10
Mercury (Hg) lamp >400 nm	RuBLRu'/Ag/TaON (Z-scheme)	MeOH	Formic acid (57 %)	Φ= 0.20 TOF= 5 h ⁻¹ TON= 41	11
Mercury (Hg) lamp >400 nm	RuRu'/Ag/TaON (Z-scheme)	Water	Formic acid (85 %)	Φ= 0.0023 TOF= 25 h ⁻¹ TON= 620	12
Mercury (Hg) lamp >400 nm	<i>trans</i> -Ru(bpy)L ₄	DMA/water (9:1)	CO (87 %) ^{b)}	TOF= 560 h ⁻¹ TON= 2,800	13
Mercury (Hg) lamp >400 nm	<i>trans</i> -Ru(bpy)L ₄	DMA/water (9:1)	CO (~80 %)	TOF= ~1,400 h ⁻¹ TON= 2,100 (5 h)	14
Xenon (Xe) lamp >400 nm	C ₃ N ₄ -RubpyL ₄	MeCN/TEOA (4:1)	Formic acid (82 %)	Φ= 0.015 TOF= 23 h ⁻¹ TON >200	15
Mercury (Hg) lamp >400 nm	C ₃ N ₄ -RubpyL ₄	DMA/TEOA (4:1)	Formic acid (>80 %)	Φ= 0.06 TOF= 141 h ⁻¹ TON= 1,100	16
Mercury (Hg) lamp >400 nm	RuRu'/Ag/C ₃ N ₄ (Z-scheme)	DMA/TEOA (4:1)	Formic acid (99 %)	Φ= 0.052 TON= 33,000 (48 h)	17
Mercury (Hg) lamp >400 nm	RuRu'/Ag/C ₃ N ₄ (Z-scheme)	10 mM K ₂ C ₂ O ₄ aqueous solution	Formic acid (83 %)	Φ= 0.052 TON= 662 (24 h)	17
Xenon (Xe) lamp >400 nm	RuRu'/Ag/C ₃ N ₄ (Z-scheme)	Na ₂ CO ₃ aqueous solution (pH 7)	Formic acid (90 %) ^{c)}	Φ= 0.2 TOF= 139 h ⁻¹ TON= 2,090	18
400 W Xe lamp >500 nm	Urea co-polymerized C ₃ N ₄ -RubpyL ₄	MeCN/TEOA (4:1)	Formic acid (98 %)	TON= 252 (5 h)	19
400 W Xe lamp >480 nm	RuRu'/Ag/Ta ₃ N ₅ (Z-scheme)	MeCN/TEOA (4:1)	Formic acid (98 %)	TON= 480 (15 h)	20

a) The performances of catalysts were calculated only for the major product; b) The maximum selectivity for carbon monoxide was 93 % with TOF of 273 h⁻¹, and TON was not provided. This result was obtained from a different reaction condition and only in early stage (30 min) of the reaction; c) The maximum selectivity for formic acid was 98% with TON of 446 in 15 h.

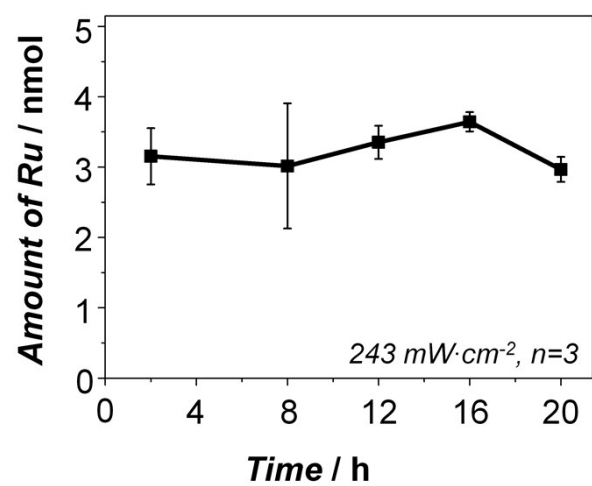


Figure S10. The amount of Ru atom after the reaction under 243 mW·cm⁻².

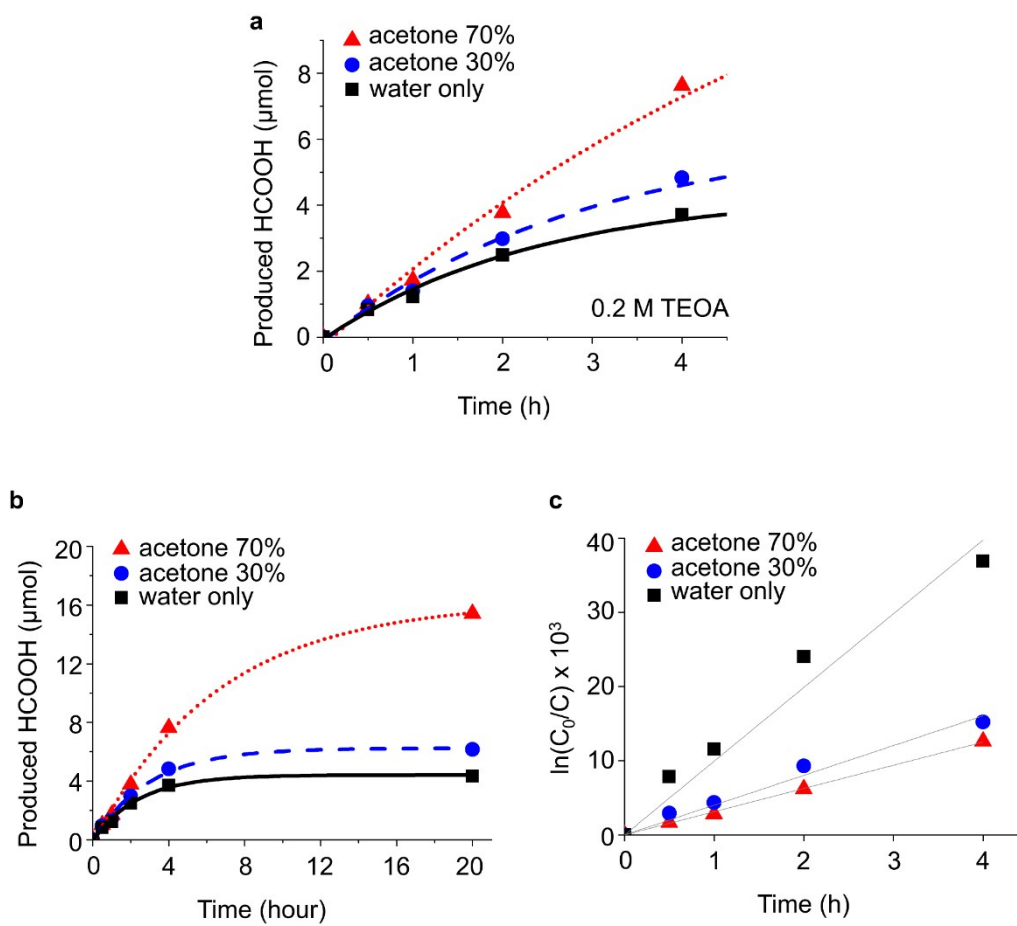


Figure S11. Formic acid production in three different solutions, containing 0%, 30%, and 70% of acetone for 4 h (a), for 20 h (b), and the calculated reaction rates up to 4 h for each solution (c).

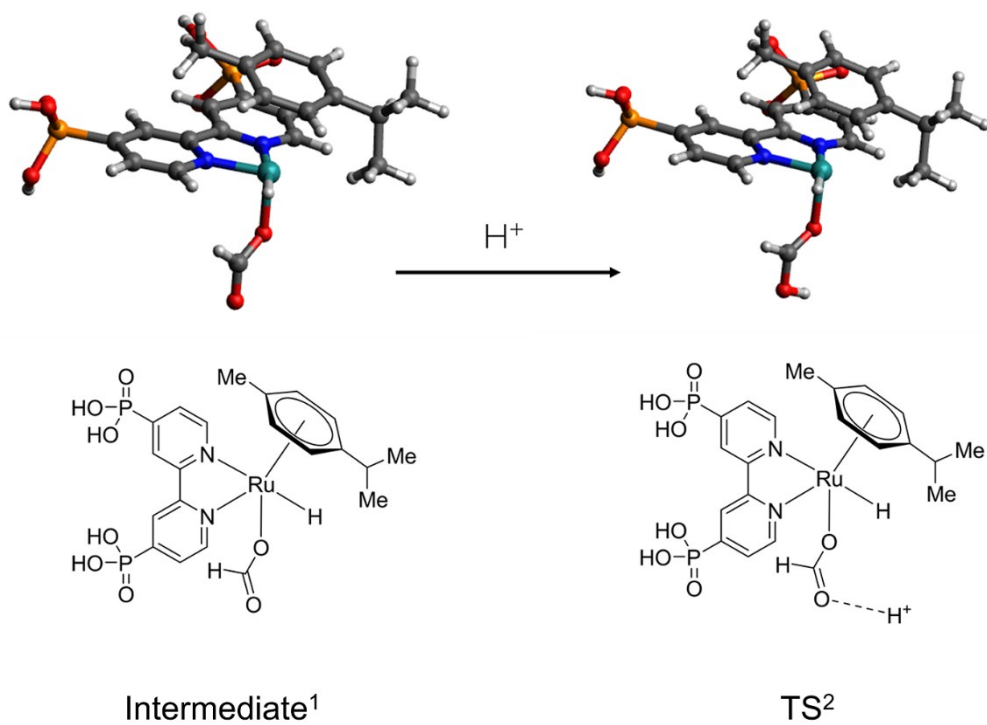


Figure S12. Chemical Structure of RuCY-formate complex at intermediate¹ and TS², calculated by using DFT (MIDI! + LanL2DZ basis set).

Table S3. The amount and selectivity of reduction products in 5 different light intensities.

Light Intensity (mW·cm ⁻²)	Reduction Product	Formic acid (μ mol, selectivity %)	Methanol	Hydrogen
60		<i>1.8997, 90.9</i>	<i>0.1530, 7.32</i>	<i>0.0372, 1.78</i>
96		<i>2.7338, 93.1</i>	<i>0.1656, 5.64</i>	<i>0.0370, 1.26</i>
120		<i>3.4525, 94.1</i>	<i>0.1728, 4.71</i>	<i>0.0437, 1.19</i>
243		<i>3.9992, 94.7</i>	<i>0.2099, 4.97</i>	<i>0.0122, 0.29</i>
360		<i>4.0497, 94.4</i>	<i>0.2094, 4.88</i>	<i>0.0309, 0.72</i>

References

- (1) T. Hirao, T. Masunaga, N. Yamada, Y. Ohshiro, T. Agawa, *Bull. Chem. Soc. Jpn.* **1982**, 55, 909-913.
- (2) M. Montalti, S. Wadhwa, W. Y. Kim, R. A. Kipp, R. H. Schmehl, *Inorg. Chem.* **2000**, 39, 76-84.
- (3) W. Kunerth, *Phys. Rev.* **1922**, 19, 512-524.
- (4) M. J. Frisch, G. W. Trucks, H. B. Schlegel, G. E. Scuseria, M. A. Robb, J. R. Cheeseman, G. Scalmani, V. Barone, B. Mennucci, G. A. Petersson, et al. Gaussian 09, *Revision A.1*, Gaussian, Inc. Wallingford CT, **2009**
- (5) Y. Zaho, D. G. Truhlar, *J. Chem. Phys.* **2006**, 125, 194101.
- (6) R. E. Easton, D. J. Giesen, A. Welch, C. J. Cramer, D. G. Truhlar, *Theor. Chim. Acta*, **1996**, 93, 281-301.
- (7) W. J. Hehre, L. Radom, P. V. R. Schleyer, J. A. Pople, *Ab Initio Molecular Orbital Theory*, Wiley, New York **1986**.
- (8) A. V. Marenich, C. J. Cramer, D. G. Truhlar, *J. Phys. Chem. B*, **2009**, 113, 6378-6396.
- (9) H. Ishida, T. Terada, K. Tanaka, T. Tanaka, *Inorg. Chem.* **1990**, 29, 905-911.
- (10) J.-M. Lehn, R. Ziessel, *J. Organomet. Chem.* **1990**, 382, 157-173.
- (11) K. Sekizawa, K. Maeda, K. Domen, K. Koike, O. Ishitani, *J. Am. Chem. Soc.* **2013**, 135, 4596-4599.
- (12) A. Nakada, T. Nakashima, K. Sekizawa, K. Maeda, O. Ishitani, *Chem. Sci.* **2016**, 7, 4364-4371.
- (13) Y. Kuramochi, J. Itabashi, K. Fukaya, A. Enomoto, M. Yoshida, H. Ishida, *Chem. Sci.* **2015**, 6, 3063-3074.
- (14) Y. Kuramochi, K. Fukaya, M. Yoshida, H. Ishida, *Chem. Eur. J.* **2015**, 21, 10049-10060.
- (15) K. Maeda, K. Sekizawa, O. Ishitani, *Chem. Commun.* **2013**, 49, 10127-10129.
- (16) R. Kuriki, K. Sekizawa, O. Ishitani, K. Maeda, *Angew. Chem. Int. Ed.* **2015**, 54, 2406-2409.

- (17) R. Kuriki, H. Matsunaga, T. Nakashima, K. Wada, A. Yamakata, O. Ishitani, K. Maeda, *J. Am. Chem. Soc.* **2016**, 138, 5159-5170.
- (18) R. Kuriki, M. Yamamoto, K. Higuchi, Y. Yamamoto, M. Akatsuka, D. Lu, S. Yagi, T. Yoshida, O. Ishitani, K. Maeda, *Angew. Chem. Int. Ed.* **2017**, 56, 4867-4871.
- (19) C. Tsounis, R. Kuriki, K. Shibata, J. J. M. Vequizo, D. Lu, A. Yamakata, O. Ishitani, R. Amai, K. Maeda, *ACS Sustainable Chem. Eng.* **2018**, 6, 15333-15340.
- (20) K. Muraoka, T. Uchiyama, D. Lu, Y. Uchimoto, O. Ishitani, K. Maeda, *Bull. Chem. Soc. Jpn.* **2019**, 92, 124-126.